Room temperature skyrmions in an exchange biased antiferromagnet

Kumari Gaurav Rana[1], Rafael Lopes Seeger[1], Sandra Ruiz-Gómez[2], Roméo Juge[1], Qiang Zhang[1], Van Tuong Pham[1], Mohamed Belmeguenai[3], Stéphane Auffret[1], Michael Foerster[2], Lucia Aballe[2], Gilles Gaudin[1], Vincent Baltz [1,*], Olivier Boulle[**,1].

1 Univ. Grenoble Alpes, CNRS, CEA, Grenoble INP***, SPINTEC, F-38000 Grenoble, France

2 Alba Synchrotron Light Facility, Carrer de la llum 2-26, 08290, Cerdanyola del Valles, Barcelona, Spain

3 Laboratoire des Sciences des Procédés et des Matériaux, CNRS, Université Paris 13, 93430 Villetaneuse, France

* vincent.baltz@cea.fr** olivier.boulle@cea.fr *** Institute of Engineering Univ. Grenoble Alpes

Abstract

Magnetic skyrmions are topological spin textures holding great potential as nanoscale information carriers. Recently, skyrmions have been predicted in antiferromagnets, with key advantages in terms of stability, size and dynamical properties over their ferromagnetic analogs. However, their experimental demonstration is lacking. Here we show that skyrmions can be stabilized at zero field and room temperature at the interface of sputtered IrMn thin films exchange-coupled to a ferromagnetic layer. This was realised by replicating the skyrmionic spin texture of the ferromagnet in the antiferromagnet, via annealing above the blocking temperature of the ferromagnet/antiferromagnet bilayer. Using the high-spatial-resolution magnetic microscopy technique XMCD-PEEM, we observe the skyrmions within the IrMn interfacial layer from the XMCD signal of the uncompensated Mn spins at the interface. This result opens up a path for logic and memory devices based on skyrmion manipulation in antiferromagnets.

Magnetic textures such as skyrmions are currently attracting a lot of attention due to their rich spin physics and their high potential for storage and logic computing. [1,2] Skyrmions are topological magnetic defects in the magnetic spin structure. [3,4] They can be found either in the bulk or interfacial systems lacking inversion symmetry, and require Dzyaloshinskii-Moriya interaction (DMI). [5–7] They hold great promise for future spintronic applications as they can be as small as few nanometers, and can be created, manipulated and annihilated electrically, in particular by an electron or a magnon flow [8,9].

Since antiferromagnets [10,11] can be magnetic at the atomic scale and non-magnetic at the macroscopic scale, skyrmions in antiferromagnets, [12,13] also known as antiferromagnetic skyrmions, may present several advantages over their ferromagnetic analogs. More specifically, they combine key features for applications in the field of spintronics as: (i) they produce no dipolar fields, making them stable at the nanometer scale in zero external magnetic field; (ii) they are robust against perturbation due to magnetic fields, which is beneficial for data retention; (iii) they exhibit zero net topological charge, [12,14] thus eliminating the unwanted transverse velocity related to the skyrmion Hall effect, [15,16] thereby ensuring a straight skyrmion trajectory with enhanced mobility. [12] However, since they lack net magnetization the experimental observation and nucleation of antiferromagnetic skyrmions is challenging. Nevertheless, direct observation of antiferromagnetic spin textures can be achieved, [17] but in large-scale facilities with element-sensitive techniques like X-ray absorption spectroscopy, [18–20] specific local probe techniques such as spin-polarized scanning tunneling microscopy [21,22] and quantum sensing with single spins (nitrogen vacancies) in diamond, [23–25] or optical second harmonic generation [26] and thermal gradient microscopy [27]. Antiferromagnetic domains and domain walls in NiO, [18,28] $BiFeO_3$, [23,26] Cr_2O_3, [24] CuMnAs [25] and Mn_3Sn [27], and vortex states in IrMn [19] and NiO [20] layers were for example investigated in those ways. The current bottleneck is the nucleation of skyrmions in antiferromagnets. Application of an external magnetic field, like in ferromagnetic [4] or synthetic antiferromagnetic [29] films, is ineffective for actual antiferromagnets. We note that, for the case of synthetic antiferromagnets, the low antiferromagnetic coupling between two ferromagnetic skyrmions makes these skyrmions sensitive to external magnetic field. An antiferromagnet is also more robust against dynamical torque deformation, since its spin structure relies on strong interatomic exchange interactions.

An alternative way to manipulate the order parameter of an antiferromagnet, is to take advantage of the strong exchange bias interaction between the antiferromagnet and an adjacent ferromagnet [30] to imprint a ferromagnetic configuration in the antiferromagnet.[11]. In a first step, exchange bias interaction is quenched by raising the sample temperature above the blocking temperature (T_B) of the ferromagnet/antiferromagnet bilayer. The antiferromagnetic layer loses its ability to pin the magnetization of the adjacent ferromagnet. The latter can then be considered as a ferromagnetic single layer in which it is possible to nucleate different types of spin textures by conventional means. In a second step, the bilayer is cooled below T_B causing the moments in the antiferromagnet to align with those of the ferromagnet due to the exchange bias coupling. This procedure was used to imprint multidomain states and magnetic textures in antiferromagnets, by

preparing the ferromagnet above T_B in specific magnetic configurations, *e.g.* multidomain states by demagnetization under decreasing, alternating magnetic field, [31,32] or vortex states by using magnetic nanostructures. [19,20]

Based on this approach, we show that magnetic skyrmions can be stabilized at zero field and room temperature in an IrMn antiferromagnet. The IrMn layer was exchange-coupled to a ferromagnetic layer hosting magnetic skyrmions. To nucleate the skyrmions in the IrMn antiferromagnet, the skyrmionic spin texture in the ferromagnet was replicated by annealing above the blocking temperature of the ferromagnetic/antiferromagnetic bilayer. Using the high spatial resolution magnetic microscopy technique XMCD-PEEM, we observe skyrmions within the IrMn layer from the XMCD signal of the uncompensated Mn spins.

The sample investigated consisted of a //Ta(3)/Cu(3)/IrMn(5)/Pt(0.5)/Co(0.3)/NiFe(0.87)/Al(2) (nm) multilayer, from substrate to surface. The polycrystalline stack was deposited at room temperature by magnetron sputtering on a $Si/SiO_2(500)$ wafer at a pressure of 2.3 x 10^{-3} mbar under argon. The IrMn antiferromagnet was deposited from an $Ir_{20}Mn_{80}$ (at. %) target and the NiFe ferromagnet was deposited from a $Ni_{81}Fe_{19}$ (at. %) permalloy target. A Ta(3)/Cu(3) seed bilayer was used to promote the growth of the antiferromagnetic (111)-textured fcc phase of the IrMn alloy. The composition of the stack was carefully optimized in order to stabilize skyrmions in both the IrMn and the Co/NiFe layer and allow for their observations using X-ray magnetic microscopy. The ultra-thin intermediate bilayer of Pt(0.5)/Co(0.3) allows us to achieve large perpendicular magnetic anisotropy as well as a large interfacial DMI [4], [33] without magnetically decoupling the IrMn and NiFe layers. This thickness of the NiFe layer was chosen in the vicinity of the planar-to-perpendicular anisotropy transition of the ferromagnet, therefore allowing us to promote the formation of skyrmions. [4] The choice of the stacking order for the IrMn and NiFe layers, combined with the reduced thickness of the NiFe layer, was such that the sensitivity of photoemission electron microscopy to Mn spins at the IrMn surface was most favorable. A 2-nm-thick Al cap, a light element, was finally deposited to form a protective and transparent $Al(2)O_x$ film after oxidation in air.

To achieve exchange bias, the sample temperature was first raised to 250°C, above T_B, [11] kept for 30 minutes and cooled to room temperature in an external magnetic field applied along the out-of-plane direction. The amplitude of the external field was of 0.57 T, *i.e.* sufficient to saturate the NiFe ferromagnetic layer. Then, the sample temperature was raised a second time to 250°C for 30 minutes at zero field and cooled to room temperature [34]. The out-of-plane magnetic-field-dependence of the Kerr signal as measured at room temperature (Fig. 1) is shifted with respect to zero-field by an exchange bias field, of around 50 mT. The linear and anhysteretic reversal of the signal further indicates stripe domain reversal.
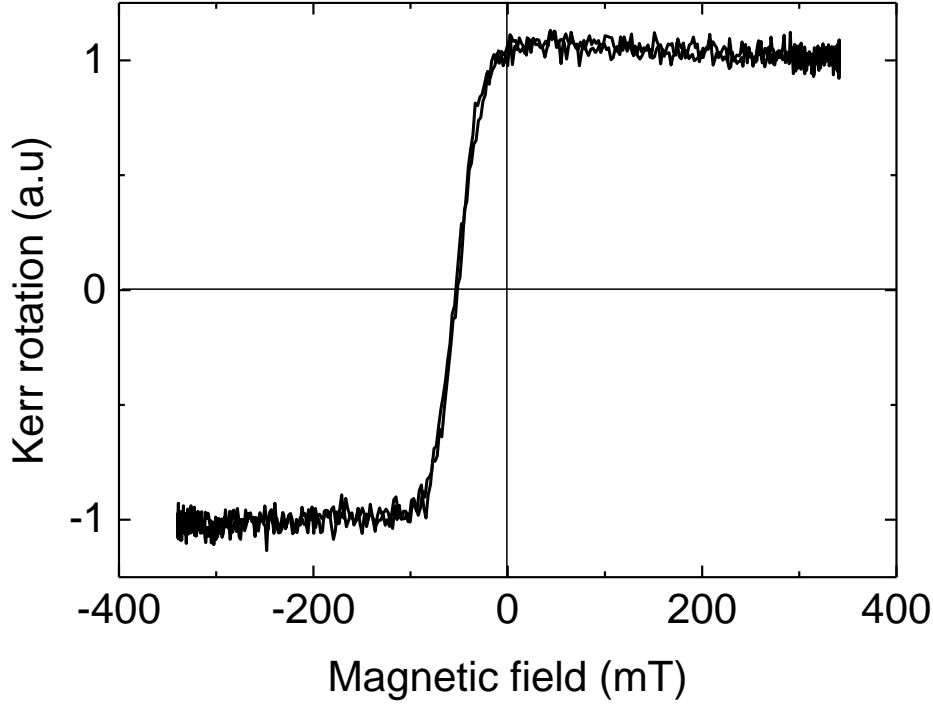
Figure 1 Out-of-plane magnetic-field-dependence of the Kerr signal as measured at room temperature for a //Ta(3)/Cu(3)/IrMn(5)/Pt(0.5)/Co(0.3)/NiFe(0.7)/Al(2) (nm) stack after the annealing procedure.

Brillouin Light Scattering experiments were carried out to extract the amplitude of the DMI which leads to $D = -0.30$ mJ/m^2 [34]. The negative value for D favors a left-handed chirality, consistently with [4,33]. The critical D associated with the Bloch to Néel domain wall transition writes [35] $D_c = 4\mu_0 M_s^2 t \ln2/2 \pi^2$ with t the film thickness . It can be estimated to be Dc=0.16 mJ/m² in our stack. Thus, $D>D_c$ and the domain wall and skyrmions are expected to be of the chiral left-handed Néel type.

To gain insight into the creation of skyrmions at the IrMn layer interface through exchange bias replication, element-specific X-ray magnetic circular dichroism photoemission electron microscopy (XMCD-PEEM) experiments were subsequently carried out at room temperature and in zero external magnetic field. These experiments were performed on the SPELEEM III microscope (Elimtec GmbH) at the CIRCE beamline in the ALBA synchrotron. [36] Typical X-ray absorption spectra (XAS) integrated over an area of about 300 µm^2 are given in Fig. 2(a) (circular polarization) and 2(b) (linear polarization). The X-ray magnetic circular dichroism (XMCD) in Fig 2(a) shows the existence of a small net magnetic moment in IrMn, ascribed to the frozen uncompensated spins after the cooling procedure. The corresponding X-ray magnetic linear

dichroism (XMLD) spectra (Fig. 2(b)) indicates that the overall orientation of the Mn spins is tilted out-of-plane, [37] in agreement with what is expected from the cooling procedure.
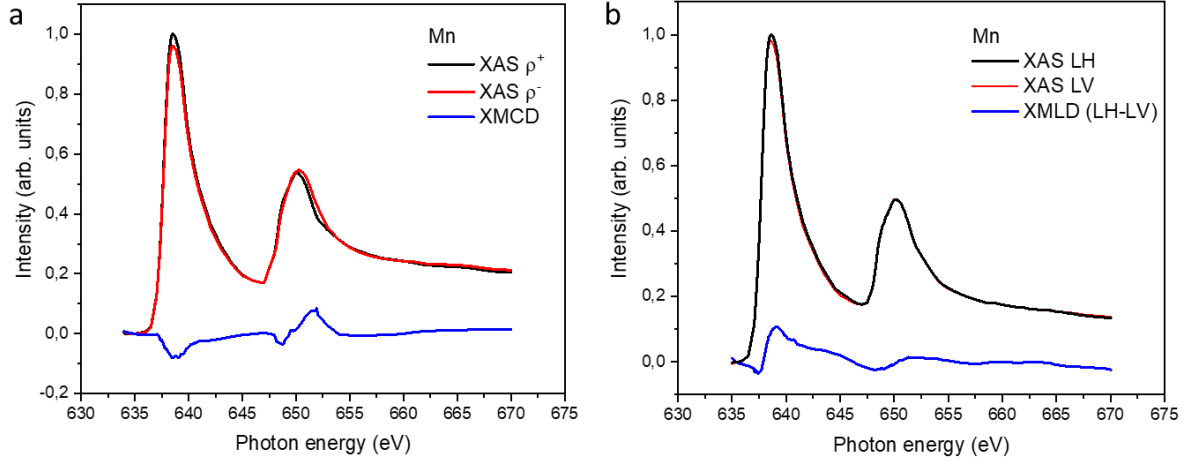

Figure 2 Energy absorption spectra corresponding to X-ray magnetic (a) circular and (b) linear dichroism photoemission electron experiments for a //Ta(3)/Cu(3)/IrMn(5)/Pt(0.5)/Co(0.3)/NiFe(0.87)/Al(2) (nm) stack. Two polarities are shown. In (a), CR and CL stands for circular right and circular left polarization respectively. XMCD is the difference of the CL and CR signal; its amplitude is multiplied by a factor 2. In (b), LH and LV stands for linear horizontal and linear vertical polarization. The energy window is focused in the vicinity of the L-edges of the Mn element.

Spatially resolved XMCD-PEEM images were recorded at the Fe, and Mn L-edges for right- and left-circularly polarized X-rays. The resulting magnetic contrast image at the Fe edge (Fig. 3(a)) indicates that magnetic skyrmions are stabilized in zero external magnetic field in the NiFe layer. Images at the Mn edge (Fig. 3(b)) provide information on the non-compensated Mn spins at the top interface of the IrMn layer. For some regions, spin textures can clearly be observed, whose shape and position coincide with the skyrmions in the NiFe ferromagnet (Fig. 3(c)). These results demonstrate that the skyrmionic spin texture in the NiFe ferromagnet is replicated in the interfacial Mn spins of the IrMn antiferromagnet. Although we cannot conclude on the penetration depth of the spin texture due to the complex spin structure of the IrMn antiferromagnet [11] combined with the weighted depth-sensitivity of the measurement, we note that earlier works have shown that exchange bias made it possible to imprint other spin textures in the depth of the antiferromagnet, down to at least 3 nm for vortices in CoO and NiO, [20] and exchange springs in IrMn [38] layers.
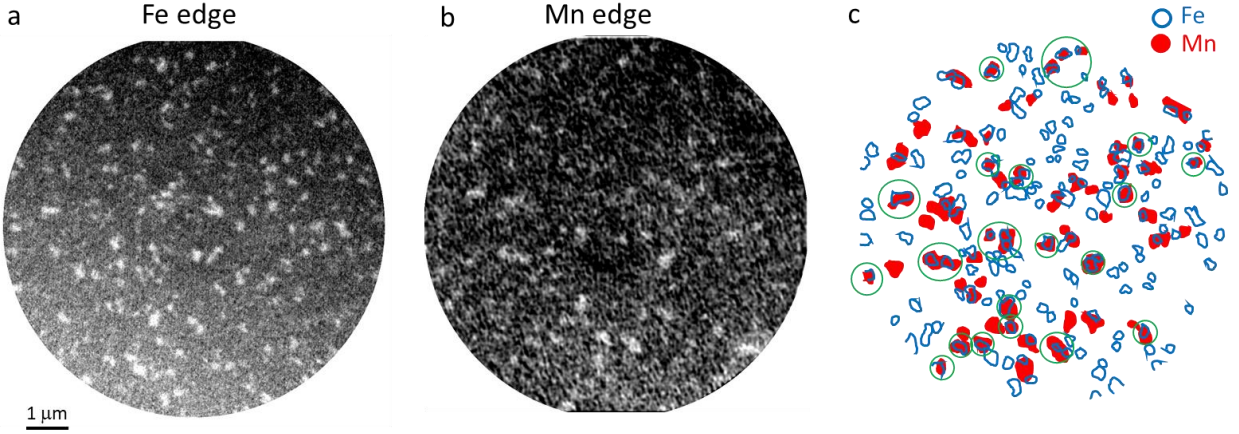
Figure 3 Images corresponding to the NiFe and IrMn magnetic contrasts for a //Ta(3)/Cu(3)/IrMn(5)/Pt(0.5)/Co(0.3)/NiFe(0.87)/Al(2) (nm) stack. The images are obtained at room temperature and in zero external magnetic field, by XMCD-PEEM at the L-edges of the energy absorption spectra of (a) the Fe and (b) the Mn elements, respectively. (c) Superposition of the contours of textures for the Fe (open, blue) and for the Mn (filled, red) elements. The green circles indicate area where an overlap between Fe and Mn skyrmions is observed.

From Fig. 3(c), we can also observe that conformity between the ferromagnetic and antiferromagnetic spin textures does not hold everywhere. For some areas, skyrmions in the NiFe layer are not replicated in the IrMn layer, and for other areas, textures in the IrMn layer are replicated but are no more facing textures in the NiFe layer. These results can be accounted for the known spatial distribution of blocking temperature (DT$_B$). [30,34,39] More specifically, for areas where $T_B \geq 300$ K, the magnetic configuration of the NiFe ferromagnet can be stabilized in the 5 nm-thick IrMn antiferromagnet at 300 K by a cooling procedure from T_B to 300 K, in contrast to areas where $T_B < 300$ K, in which case, textures cannot be stabilized in this way in the IrMn antiferromagnet. [40,41] Note that there has been so far only indirect insights on such spatial distributions, for example through the correlation between disordered magnetic phases spread above ferromagnetic/antiferromagnetic thin films and device-to-device variability of exchange bias in spintronic applications, after patterning the thin film. [42] Here, our observation would provide a direct observation of spatial distribution of blocking temperature in an exchange-biased stack.

In conclusion, we demonstrate the stabilization of skyrmions at the interface of a sputtered IrMn antiferromagnetic thin film, at room temperature and in zero external magnetic field. The skyrmions were nucleated by replicating the skyrmionic spin texture of an adjacent exchange biased ferromagnet by annealing above the blocking temperature of the ferromagnet/antiferromagnet bilayer. Element-specific X-ray magnetic microscopy allows the direct observation of the skyrmionic spin texture at the interface of the antiferromagnet, from the

uncompensated Mn spins at the interface. This study paves the way for future advances, since several spin-dependent transport effects in antiferromagnetic skyrmions, like topological Hall [43] or spin-orbit torque [44] effects, have been theoretically predicted and have yet to be experimentally demonstrated, along with the closely related promising applications opening up a path for logic and memory devices based on skyrmion manipulation in antiferromagnets..

Acknowledgement

References

[1] S. S. P. Parkin, M. Hayashi, and L. Thomas, *Magnetic Domain-Wall Recetrack Memory*, Science **320**, 190 (2008).

[2] A. Fert, V. Cros, and J. Sampaio, *Skyrmions on the Track*, Nat. Nanotechnol. **8**, 152 (2013).

[3] U. K. Rößler, A. N. Bogdanov, and C. Pfleiderer, *Spontaneous Skyrmion Ground States in Magnetic Metals*, Nature **442**, 797 (2006).

[4] O. Boulle, J. Vogel, H. Yang, S. Pizzini, D. de Souza Chaves, A. Locatelli, T. O. Menteş, A. Sala, L. D. Buda-Prejbeanu, O. Klein, M. Belmeguenai, Y. Roussigné, A. Stashkevich, S. M. Chérif, L. Aballe, M. Foerster, M. Chshiev, S. Auffret, I. M. Miron, and G. Gaudin, *Room-Temperature Chiral Magnetic Skyrmions in Ultrathin Magnetic Nanostructures*, Nat. Nanotechnol. **11**, 449 (2016).

[5] I. Dzyaloshinskii, *Thermodynamic Theory of "weak" Ferromagnetism of Antiferromagnetics*, J. Phys. Chem. Solids **4**, 241 (1958).

[6] T. Moriya, *Anisotropic Superexchange and Weak Ferromagnetism*, Phys Rev **120**, 91 (1960).

[7] A. Fert and P. M. Levy, *Role of Anisotropic Exchange Interactions in Determining the Properties of Spin-Glasses*, Phys Rev Lett **44**, 1538 (1980).

[8] N. Nagaosa and Y. Tokura, *Topological Properties and Dynamics of Magnetic Skyrmions*, Nat. Nanotechnol. **8**, 899 (2013).

[9] A. Fert, N. Reyren, and V. Cros, *Magnetic Skyrmions: Advances in Physics and Potential Applications*, Nat Rev Mater **2**, 17031 (2017).

[10] T. Jungwirth, X. Marti, P. Wadley, and J. Wunderlich, *Antiferromagnetic Spintronics*, Nat. Nanotechnol. **11**, 231 (2016).

[11] V. Baltz, A. Manchon, M. Tsoi, T. Moriyama, T. Ono, and Y. Tserkovnyak, *Antiferromagnetic Spintronics*, Rev Mod Phys **90**, 015005 (2018).

[12] J. Barker and O. A. Tretiakov, *Static and Dynamical Properties of Antiferromagnetic Skyrmions in the Presence of Applied Current and Temperature*, Phys Rev Lett **116**, 147203 (2016).

[13] O. Gomonay, V. Baltz, A. Brataas, and Y. Tserkovnyak, *Antiferromagnetic Spin Textures and Dynamics*, Nat. Phys. **14**, 213 (2018).

[14] L. Šmejkal, Y. Mokrousov, B. Yan, and A. H. MacDonald, *Topological Antiferromagnetic Spintronics*, Nat. Phys. **14**, 242 (2018).

[15] W. Jiang, X. Zhang, G. Yu, W. Zhang, X. Wang, B. M. Jungfleich, J. E. Pearson, X. Cheng, O. Heinonen, K. L. Wang, Y. Zhou, A. Hoffmann, and S. G. E. te Velthuis, *Direct Observation of the Skyrmion Hall Effect*, Nat. Phys. **13**, 162 (2017).

[16] R. Juge, S.-G. Je, D. de Souza Chaves, L. D. Buda-Prejbeanu, J. Peña-Garcia, J. Nath, I. M. Miron, K. G. Rana, L. Aballe, M. Foerster, F. Genuzio, T. O. Mente, A. Locatelli, F. Maccherozzi, S. S. Dhesi, M. Belmeguenai, Y. Roussigné, S. Auffret, S. Pizzini, G. Gaudin, J. Vogel, and O. Boulle, *Current-Driven Skyrmion Dynamics and Drive-Dependent Skyrmion Hall Effect in an Ultrathin Film*, Phys Rev Appl. **12**, 44007 (2019).

[17] S.-W. Cheong, M. Fiebig, W. Wu, L. Chapon, and V. Kiryukhin, *Seeing Is Believing: Visualization of Antiferromagnetic Domains*, Npj Quantum Mater. **5**, 3 (2020).

[18] N. B. Weber, H. Ohldag, H. Gomonaj, and F. U. Hillebrecht, *Magnetostrictive Domain Walls in Antiferromagnetic NiO.*, Phys. Rev. Lett. Lett. **91**, 237205 (2003).

[19] G. Salazar-Alvarez, J. J. Kavich, J. Sort, A. Mugarza, S. Stepanow, A. Potenza, H. Marchetto, S. S. Dhesi, V. Baltz, B. Dieny, A. Weber, L. J. Heyderman, J. Nogues, and P. Gambardella, *Direct Evidence of Imprinted Vortex States in the Antiferromagnet of Exchange Biased Microdisks*, Appl. Phys. Lett. **95**, 012510 (2009).

[20] J. Wu, D. Carlton, J. S. Park, Y. Meng, E. Arenholz, A. Doran, A. T. Young, A. Scholl, C. Hwang, H. W. Zhao, J. Bokor, and Z. Q. Qiu, *Direct Observation of Imprinted Antiferromagnetic Vortex States in CoO/Fe/Ag(001) Discs*, Nat. Phys. **7**, 303 (2011).

[21] M. Bode, E. Y. Vedmedenko, K. von Bergmann, A. Kubetzka, P. Ferriani, S. Heinze, and R. Wiesendanger, *Atomic Spin Structure of Antiferromagnetic Domain Walls*, Nat. Mater. **5**, 477 (2006).

[22] S. Loth, S. Baumann, C. P. Lutz, D. M. Eigler, and A. J. Heinrich, *Bistability in Atomic-Scale Antiferromagnets*, Science **335**, 196 (2012).

[23] I. Gross, W. Akhtar, V. Garcia, L. J. Martínez, S. Chouaieb, K. Garcia, C. Carrétéro, A. Barthélémy, P. Appel, P. Maletinsky, J.-V. Kim, J. Y. Chauleau, N. Jaouen, M. Viret, M. Bibes, S. Fusil, and V. Jacques, *Real-Space Imaging of Non-Collinear Antiferromagnetic Order with a Single Spin Magnetometer*, Nature **549**, 252 (2017).

[24] T. Kosub, M. Kopte, R. Hu, P. Appel, B. Shields, P. Maletinsky, O. G. Schmidt, and D. Makarov, *Purely Antiferromagnetic Magnetoelectric Random Access Memory*, Nat. Commun. **8**, 13985 (2017).

[25] M. S. Wörnle, P. Welter, Z. Kašpar, K. Olejník, V. Novák, R. P. Campion, P. Wadley, T. Jungwirth, C. L. Degen, and P. Gambardella, *Current-Induced Fragmentation of Antiferromagnetic Domains*, ArXiv:1912.05287 (2019).

[26] J.-Y. Chauleau, E. Haltz, C. Carrétéro, S. Fusil, and M. Viret, *Multi-Stimuli Manipulation of Antiferromagnetic Domains Assessed by Second-Harmonic Imaging*, Nat. Mater. **16**, 803 (2017).

[27] H. Reichlova, T. Janda, J. Godinho, A. Markou, D. Kriegner, R. Schlitz, J. Zelezny, Z. Soban, M. Bejarano, H. Schultheiss, P. Nemec, T. Jungwirth, C. Felser, J. Wunderlich, and S. T. B. Goennenwein, *Imaging and Writing Magnetic Domains in the Non-Collinear Antiferromagnet Mn3Sn*, Nat. Commun. **10**, 5459 (2019).

[28] M. Fiebig, D. Fröhlich, Th. Lottermoser, V. V. Pavlov, R. V. Pisarev, and H.-J. Weber, *Second Harmonic Generation in the Centrosymmetric Antiferromagnet NiO*, Phys. Rev. Lett. **87**, 137202 (2001).

[29] W. Legrand, D. Maccariello, F. Ajejas, S. Collin, A. Vecchiola, K. Bouzehouane, N. Reyren, V. Cros, and A. Fert, *Room-Temperature Stabilization of Antiferromagnetic Skyrmions in Synthetic Antiferromagnets*, Nat. Mater. **19**, 34 (2020).

[30] J. Nogués and I. K. Schuller, *Exchange Bias*, J. Magn. Magn. Mater. **192**, 203 (1999).

[31] S. Brück, J. Sort, V. Baltz, S. Suriñach, J. S. Muñoz, B. Dieny, M. D. Baró, and J. Nogués, *Exploiting Length Scales of Exchange-Bias Systems to Fully Tailor Double-Shifted Hysteresis Loops*, Adv. Mater. **17**, 2978 (2005).

[32] I. V. Roshchin, O. Petracic, R. Morales, Z.-P. Li, X. Batlle, and I. K. Schuller, *Lateral Length Scales in Exchange Bias*, Europhys. Lett. EPL **71**, 297 (2005).

[33] K. G. Rana, A. Finco, F. Fabre, S. Chouaieb, A. Haykal, L. D. Buda-Prejbeanu, O. Fruchart, S. Le Denmat, P. David, M. Belmeguenai, T. Denneulin, R. E. Dunin-Borkowski, G. Gaudin, V. Jacques, and O. Boulle, *Room Temperature Skyrmions at Zero Field in Exchange-Biased Ultrathin Films*, Phys Rev Appl. **13**, 044079 (2020).

[34] *See Supplemental Material*, (n.d.).

[35] A. Thiaville, S. Rohart, É. Jué, V. Cros, and A. Fert, *Dynamics of Dzyaloshinskii Domain Walls in Ultrathin Magnetic Films*, EPL Europhys. Lett. **100**, 57002 (2012).

[36] L. Aballe, M. Foerster, E. Pellegrin, J. Nicolas, and S. Ferrer, *The ALBA Spectroscopic LEEM-PEEM Experimental Station: Layout and Performance*, J. Synchrotron Radiat. **22**, 745 (2015).

[37] Y. Y. Wang, C. Song, G. Y. Wang, F. Zeng, and F. Pan, *Evidence for Asymmetric Rotation of Spins in Antiferromagnetic Exchange-Spring*, New J. Phys. **16**, 123032 (2014).

[38] H. Reichlová, V. Novák, Y. Kurosaki, M. Yamada, H. Yamamoto, A. Nishide, J. Hayakawa, H. Takahashi, M. Maryško, J. Wunderlich, X. Marti, and T. Jungwirth, *Temperature and Thickness Dependence of Tunneling Anisotropic Magnetoresistance in Exchange-Biased Py/IrMn/MgO/Ta Stacks*, Mater. Res. Express **3**, 076406 (2016).

[39] V. Baltz, B. Rodmacq, A. Zarefy, L. Lechevallier, and B. Dieny, *Bimodal Distribution of Blocking Temperature in Exchange-Biased Ferromagnetic/Antiferromagnetic Bilayers*, Phys. Rev. B **81**, 052404 (2010).

[40] V. Baltz, J. Sort, B. Rodmacq, B. Dieny, and S. Landis, *Thermal Activation Effects on the Exchange Bias in Ferromagnetic-Antiferromagnetic Nanostructures*, Phys. Rev. B **72**, 104419 (2005).

[41] G. Lhoutellier, D. Ledue, R. Patte, F. Barbe, B. Dieny, and V. Baltz, *Bimodal Distribution of Blocking Temperature for Exchange-Bias Ferromagnetic/Antiferromagnetic Bilayers: A Granular Monte Carlo Study with Less Stable Magnetic Regions Spread over the Interface*, J. Phys. Appl. Phys. **48**, 115001 (2015).

[42] K. Akmaldinov, L. Frangou, C. Ducruet, C. Portemont, J. Pereira, I. Joumard, B. Dieny, J. Alvarez-Hérault, and V. Baltz, *Disordered Magnetic Phases Located over Ferromagnetic/Antiferromagnetic Films Impact on Cell-to-Cell Variability of Exchange Bias in Thermally-Assisted MRAM Chips*, IEEE Magn. Lett. **6**, 3000404 (2015).

[43] C. A. Akosa, O. A. Tretiakov, G. Tatara, and A. Manchon, *Theory of the Topological Spin Hall Effect in Antiferromagnetic Skyrmions: Impact on Current-Induced Motion*, Phys. Rev. Lett. **121**, 97204 (2018).

[44] C. Jin, C. Song, J. Wang, and Q. Liu, *Dynamics of Antiferromagnetic Skyrmion Driven by the Spin Hall Effect*, Appl. Phys. Lett. **109**, 182404 (2016).

[45] M. Belmeguenai, J.-P. Adam, Y. Roussigné, S. Eimer, T. Devolder, J.-V. Kim, S. M. Cherif, A. Stashkevich, and A. Thiaville, *Interfacial Dzyaloshinskii-Moriya Interaction in*

Perpendicularly Magnetized ${\text{Pt/Co/AlO}}_{x}$ Ultrathin Films Measured by Brillouin Light Spectroscopy, Phys. Rev. B **91**, 180405 (2015).

[46] J. Nogués and I. K. Schuller, *Exchange Bias*, J. Magn. Magn. Mater. **192**, 203 (1999).

[47] S. Soeya, T. Imagawa, K. Mitsuoka, and S. Narishige, *Distribution of Blocking Temperature in Bilayered Ni81Fe19/NiO Films*, J. Appl. Phys. **76**, 5356 (1994).

[48] V. Baltz, B. Rodmacq, A. Zarefy, L. Lechevallier, and B. Dieny, *Bimodal Distribution of Blocking Temperature in Exchange-Biased Ferromagnetic/Antiferromagnetic Bilayers*, Phys. Rev. B **81**, 052404 (2010).

[49] G. Lhoutellier, D. Ledue, R. Patte, F. Barbe, B. Dieny, and V. Baltz, *Bimodal Distribution of Blocking Temperature for Exchange-Bias Ferromagnetic/Antiferromagnetic Bilayers: A Granular Monte Carlo Study with Less Stable Magnetic Regions Spread over the Interface*, J. Phys. Appl. Phys. **48**, 115001 (2015).

[50] E. Fulcomer and S. H. Charap, *Thermal Fluctuation Aftereffect Model for Some Systems with Ferromagnetic-antiferromagnetic Coupling*, J. Appl. Phys. **43**, 4190 (1972).

[51] K. Takano, R. H. Kodama, A. E. Berkowitz, W. Cao, and G. Thomas, *Role of Interfacial Uncompensated Antiferromagnetic Spins in Unidirectional Anisotropy in Ni81Fe19/CoO Bilayers (Invited)*, J. Appl. Phys. **83**, 6888 (1998).

Supplemental material

1. Determination of the Dzyaloshinskii-Moriya interaction using Brillouin light scattering experiments

To extract the Dzyaloshinskii-Moriya interaction (DMI), we carried out Brillouin light scattering experiments. The principle of the technique is the following [45]: the magnetisation is saturated in the film plane by an external magnetic field and spin waves (SW) propagating along the direction perpendicular to this field are probed by a laser with a well-defined wave vector k_{SW}. The DMI introduces a preferred handedness and therefore leads to an energy difference between two SW propagating with opposite wave vectors. This energy difference corresponds to a shift in frequency : $\Delta f (k_{SW}) = f_S (k_{SW}) - f_{AS} (k_{SW})$ where f_S and f_{AS} are the Stokes (a SW is created) and Anti-Stokes (a SW was absorbed) frequencies respectively. This frequency shift is directly related to the DMI value D [45]: $\Delta f(k_{SW}) = 2\gamma k_{SW}D/(\pi Ms)$ with γ the gyromagnetic ratio. Figure S1(a) shows the frequency of the Stokes and Anti-stokes peaks as a function of k_{SW} performed for several wave vectors. The shift in frequency $\Delta f = f_S - f_{AS}$ scales linearly with k_{SW} (Figure S1(b)), which allows us to extract $D = -0.30$ mJ/m^2 using $Ms_{eff} = 8.73 \times 10^5$ A.m^{-1} measured separately by SQUID magnetometry and $\gamma /(2\pi) = 31$ GHz/T. In these Brillouin light scattering experiments, a negative value for D indicates a left-handed chirality, consistently with our previous work [4,33]. The critical D associated with the Bloch to Néel domain wall transition writes [35] $D_c=4\mu_0 Ms^2 t$

ln2/2 π^2 with t the film thickness, which can be estimated to be Dc=0.16 mJ/m² in our stack. Thus, D>D_c and the domain wall and skyrmions in our samples are expected to be of the chiral left handed Néel type.
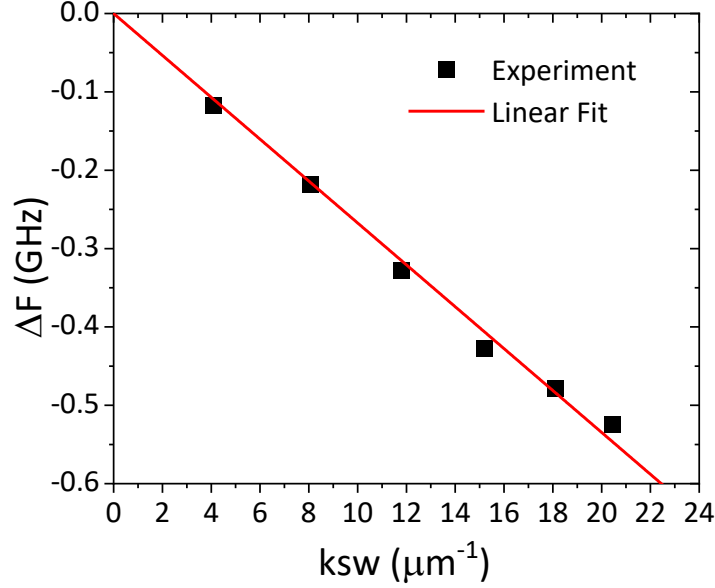

Figure S1 Frequency shift Δf versus the in-plan kvector k_{SW} for an in-plane field of μ_0H=0.8T as a result of Brillouin light scattering experiments for a //Ta(3)/Cu(3)/IrMn(5)/Pt(0.5)/Co(0.3)/NiFe(0.87)/Al(2) (nm) multilayer.

2. Additional XMCD-PEEM experiments

a. Effect of an external magnetic field

We also studied how the application of an external magnetic field affects the spin texture in both the ferromagnet and the antiferromagnet. The application of a small magnetic field (μ_0H_z=7mT) applied perpendicularly to the film plane results in the formation of larger white domains and skyrmions in the NiFe layer (see Figure S2). Interestingly, we observe that the domains in the non-compensated Mn spins at the interface are also affected by the changes in the domains in the NiFe layer: larger white domains are observed at the XMCD L3 Mn edge as compared to the zero field case. As known in the field of exchange bias, when exchange coupling is large compared to other energy terms like anisotropy, the non-compensated spins in the antiferromagnet are dragged by the spins in the ferromagnet upon application of an external field [46]. This finding confirms that exchange bias plays a significant role in the stabilization of skyrmion spin texture.
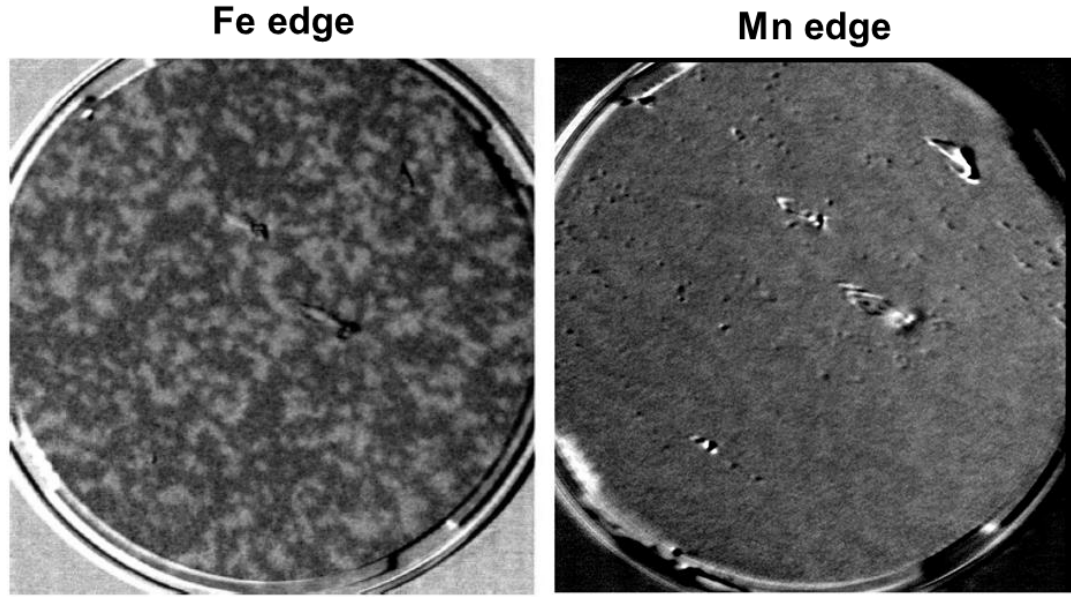
Figure S2 XMCD-PEEM image at room temperature field of a //Ta(5)/Cu(3)/IrMn(5)/Pt(0,5)/Co(0,3)/NiFe(0.7)/Al(2) (thickness in nm) measured at the L3 Fe edge and the L3 Mn edge under a perpendicular field of 7 mT.

b. Influence of the annealing procedure

In the sample described in the main text, the skyrmionic spin texture in the ferromagnet was nucleated in the antiferromagnet using a two step annealing procedure. In the first annealing, the sample was heated above the maximum blocking temperature of the antiferromagnet (see main text and section 3 below) in a large external magnetic field in order to achieve exchange bias and create skyrmions in the ferromagnetic layer. The sample was then annealed a second time above the maximum blocking temperature and cooled down under zero external magnetic field, with the idea of replicating the skyrmionic spin texture in the antiferromagnet.

  To clarify the influence of the annealing procedure on the skyrmion nucleation, we prepared   a IrMn(5)/Pt(0.5)/Co(0.3)/NiFe(0.59) (nm) sample where we carried out only the first field cooled annealing step. XMCD-PEEM imaging at the L3 Fe edge shows the stabilization of large domains as well as magnetic skyrmions at zero field in the NiFe layer (Figure S3b). Images at the L3 Mn edge shows a very similar spin texture demonstrating that the domain and skyrmions in the ferromagnetic layer are replicated in the interfacial non compensated Mn spins (Figure S3c). This demonstrates that the second annealing, followed by zero field cooling, is not required to replicate the skyrmions in the IrMn. This points to the role of the exchange interaction with the ferromagnetic layer in the stabilization of the spin texture and skyrmions in the Mn.

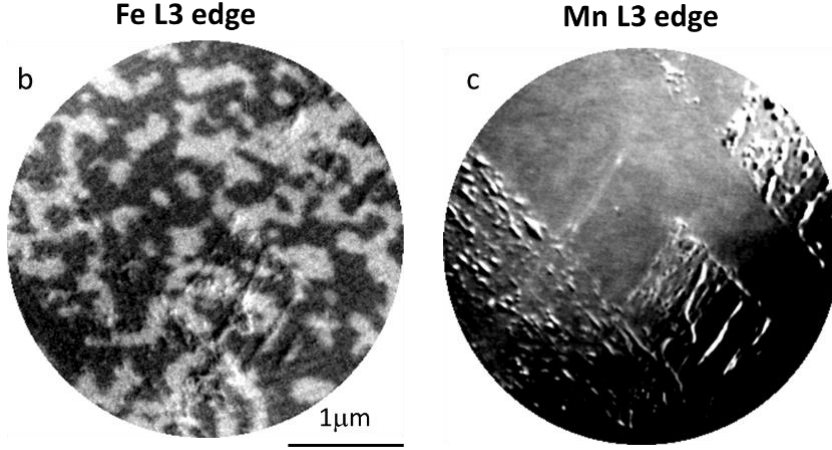**Fe L3 edge**   **Mn L3 edge**

1μm

Figure S3   a-b. XMCD-PEEM image measured at zero field and room temperature at the Fe L3 edge (b) and Mn L3 edge (c). The sample is composed of a //Ta(3)Cu(3)/IrMn(5)/Pt(0,5)/Co(0,3)/NiFe(0.59)/Al(2) (thickness in nm) multilayer deposited by magnetron sputtering on a Si wafer. The sample was heated above the blocking temperature of the AFM (at 250°C for 30 minutes) and then cooled in a large external magnetic field (0.57 T) applied perpendicularly to the film plane.

3. Blocking temperature distribution

The blocking temperature (T_B) distribution of the //Ta(3)/Cu(3)/IrMn(5)/Pt(0.5)/Co(0.3)/NiFe(0.87)/Al(2) (nm) multilayer was experimentally measured (Fig. S4) using a standard stepwise procedure [47–49].
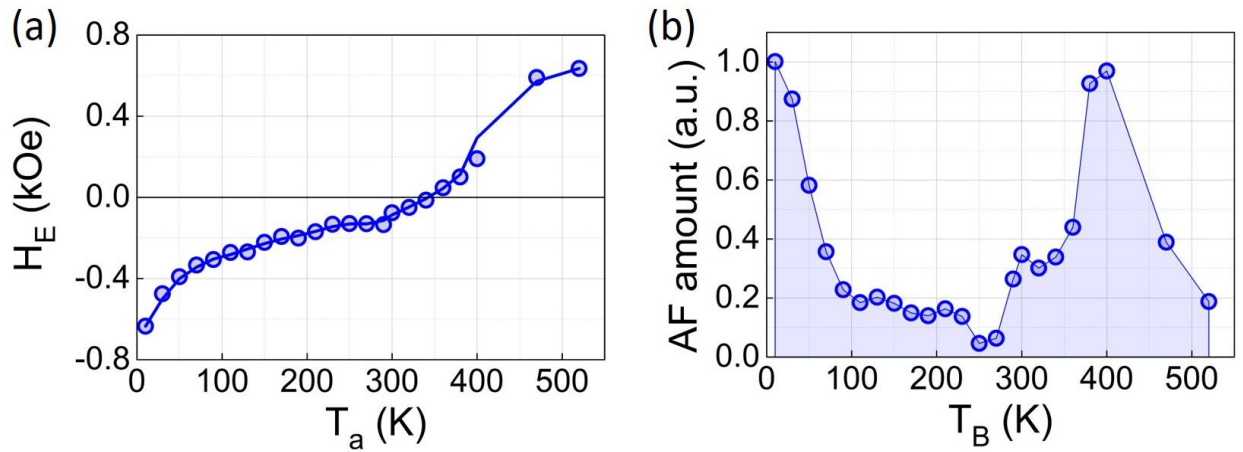

Figure S4 (a) Variation of H_E vs. T_a for a //Ta(3)/Cu(3)/IrMn(5)/Pt(0.5)/Co(0.3)/NiFe(0.87)/Al(2) (nm) multilayer.. The full line is a smooth interpolation of the data. (b) Blocking temperature distribution, corresponding to the derivative dHE/dTa vs. Ta from the data interpolation.

13

In this standard procedure, the sample is first field-cooled from above the maximum blocking temperature (here, 520 K) down to 10 K under a positive field. This cooling causes the magnetic phases of the IrMn antiferromagnetic (AF) layer in contact with the ferromagnetic layer to align in the positive direction. Then, the sample's temperature is raised to an intermediate annealing temperature, T_a, and the sample is subsequently field-cooled under a negative field down to 10 K. This cooling step results in a negative reorientation of the magnetic phases of the antiferromagnetic layer in contact with the ferromagnet when the blocking temperature is lower than T_a. Finally, a hysteresis loop is measured at 10 K. These steps are repeated for a range of T_a and the variation in the exchange field, H_E, with T_a is recorded (Figure S4(a)). Since the increase in the exchange field with T_a is related to the negative repolarization of the magnetic phases of the antiferromagnetic layer, the derivative, dH_E/dT_a (Figure S4(b)) is linked to the blocking temperature distributions of these magnetic phases [47–49].

It is acknowledged that the volume distribution of grains in the antiferromagnet in direct contact with the ferromagnet gives rise to a high-temperature peak [48–50], and that additional magnetically frustrated phases spatially distributed over the interface result in a low-temperature contribution [48,49,51]. Most importantly, the results shown in (Figure S4(b)) indicate that the blocking temperatures of the various areas composing the IrMn/NiFe interface are distributed on both sides of 300 K. As a result, for areas where $T_B \geq 300$ K, the magnetic configuration of the NiFe ferromagnet can be stabilized in the IrMn antiferromagnet at 300 K by a cooling procedure from T_B to 300 K, in contrast to areas where $T_B < 300$ K.